4-15-2016

Basal characteristics of the main sticky spot on the ice plain of Whillans Ice Stream, Antarctica

Tarun Luthra
The Pennsylvania State University

Sridhar Anandakrishnan
The Pennsylvania State University

J. Paul Winberry
Central Washington University, winberry@geology.cwu.edu

Richard B. Alley
The Pennsylvania State University

Nicholas Holschuh
The Pennsylvania State University

Recommended Citation

Luthra, T., Anandakrishnan, S., Winberry, J. P., Alley, R. B., & Holschuh, N. (2016). Basal characteristics of the main sticky spot on the ice plain of Whillans Ice Stream, Antarctica. *Earth and Planetary Science Letters 440,* 12–19. https://doi.org/10.1016/j.epsl.2016.01.035

Earth and Planetary Science Letters 440 (2016) 12–19

Contents lists available at ScienceDirect

Earth and Planetary Science Letters

www.elsevier.com/locate/epsl

Basal characteristics of the main sticky spot on the ice plain of Whillans Ice Stream, Antarctica

Tarun Luthra [a,*], Sridhar Anandakrishnan [a], J. Paul Winberry [b], Richard B. Alley [a], Nicholas Holschuh [a]

[a] Department of Geosciences, Pennsylvania State University, University Park, PA, USA
[b] Department of Geological Sciences, Central Washington University, Ellensburg, WA, USA

ARTICLE INFO

Article history:
Received 5 November 2015
Received in revised form 28 January 2016
Accepted 31 January 2016
Available online 12 February 2016
Editor: P. Shearer

Keywords:
West Antarctic Ice Sheet
geophysics
glaciology
Whillans Ice Stream
sticky spot
reflection seismology

ABSTRACT

Understanding the processes that affect streaming ice flow and the mass balance of glaciers and ice sheets requires sound knowledge of their subglacial environments. Previous studies have shown that an extensive deformable subglacial sediment layer favors fast ice-stream flow. However, areas of high basal drag, termed sticky spots, are of particular interest because they inhibit the fast flow of the overriding ice. The stick-slip behavior of Whillans Ice Stream (WIS) is perhaps the most conspicuous manifestation of a subglacial sticky spot. We present new ice-thickness and seismic-reflection measurements collected over the main sticky spot in the ice plain of WIS, allowing us to elucidate its role in the behavior of the ice stream. Ice-thickness and surface-elevation data show that the sticky spot occupies a subglacial topographic high. Water flow in response to the hydrological potential gradient will be routed around the sticky spot if effective pressures are similar on the sticky spot and elsewhere. The seismic experiment imaged a laterally continuous basal layer approximately 6 m thick, having compressional wave velocities of greater than 1800 $m\,s^{-1}$ and density greater than 1800 $kg\,m^{-3}$, indicative of a till layer that is stiffer than corresponding till beneath well-lubricated parts of the ice stream. This layer likely continues to deform under the higher shear stress of the sticky spot, and some water may be pumped up onto the sticky spot during motion events.

1. Introduction

The West Antarctic Ice Sheet (WAIS) has been losing mass at an increasing rate, contributing to sea-level rise (Joughin and Alley, 2011; Joughin et al., 2014). Ice draining into the Amundsen Sea has accelerated in response to loss of ice-shelf buttressing caused by warmer waters intruding beneath ice shelves and melting them from below (Jacobs et al., 2011). Additional mass loss is likely (Rignot et al., 2014; Joughin et al., 2014), with the potential for marine regions to raise sea level more than 3 m (Bamber et al., 2009).

In contrast, some of the ice streams of the Ross Sea drainage basin have thickened over the last century, offsetting part of the mass loss in the Amundsen Sea drainage that dominates the modern West Antarctic mass balance signal. Kamb Ice Stream slowed about 150 yrs ago (Engelhardt and Kamb, 2013), and Whillans Ice Stream is now slowing (Joughin et al., 2005; Beem et al., 2014; Winberry et al., 2014). These changes do not appear to have been forced from the Ross Ice Shelf; rather, hypotheses for the slowdown generally invoke changes in basal conditions in response to internal instabilities or long-term climate forcing (Anandakrishnan and Alley, 1997; Tulaczyk et al., 2000; Winberry et al., 2014).

The Ross Ice Streams flow rapidly under very low driving stress, with strong lubrication from subglacial till containing high-pressure water, which provides a smooth and deformable bed (Blankenship et al., 1986; Alley et al., 1986, 1987; Kamb, 2001). Even small changes in water pressure or till porosity can have large influence on this lubrication (Clarke, 1987; Tulaczyk et al., 2000). The record of flow in the Ross Ice Shelf shows strong, persistent but non-uniform variability of flow speeds of the Siple Coast ice streams (Hulbe and Fahnestock, 2007), likely because of changing basal lubrication of the ice streams.

Where large areas of the Siple Coast ice stream beds are well-lubricated, resistance comes primarily from side drag (Raymond et al., 2001) and from "sticky spots" (MacAyeal, 1989). These restricted regions of anomalously high drag are analogous to asperities on tectonic faults, and may have many origins, including till discontinuity or till dewatering (Alley, 1993).

* Corresponding author.
E-mail address: tyl5106@psu.edu (T. Luthra).

http://dx.doi.org/10.1016/j.epsl.2016.01.035

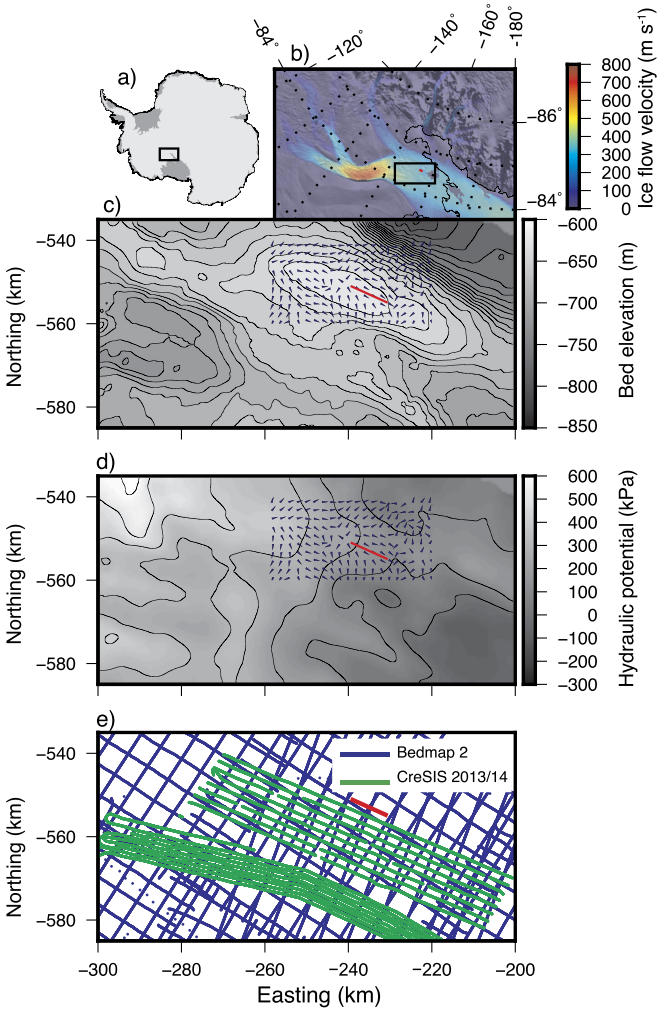

Fig. 1. a) Location of Whillans Ice Stream seismic profile. b) Ice-flow velocity of WIS (Rignot et al., 2011), together with box showing location of panels c–e. c) Bed elevation (contour interval 10 m; highest contour −620 m), hydrologic potential flowlines (black arrows), and, the seismic profile (red line), which is oriented parallel to ice-stream flow. d) As in panel c, but showing hydrologic potential. Contour interval 100 kPa; highest contour 600 kPa. e) Flight lines for Bedmap2 (blue) and new CReSIS data (green). (For interpretation of the references to color in this figure legend, the reader is referred to the web version of this article.)

Interest in sticky spots has been heightened by the discovery of their role in the stick-slip motion of the Whillans "ice plain", the downglacier-most ∼150 km of the ice stream before it enters the Ross Ice Shelf (Bindschadler et al., 2003) GPS position data showed that the ice stream completed almost all of its displacement in two rapid-motion events per day, one just after high tide in the Ross Sea, and one just before low tide (Bindschadler et al., 2003; Winberry et al., 2009, 2011, 2013, 2014). Each slip event produces far-field seismic energy (Wiens et al., 2008) linked to breakage of sticky spots (Pratt et al., 2014). Three sticky spots near the grounding line (Pratt et al., 2014; Winberry et al., 2014), possibly caused by till compaction arising from tidal flexure of the ice shelf (Walker et al., 2013), contribute to the generation of seismic energy, but a central sticky spot appears to be more important in restraining ice motion and triggering motion events (Winberry et al., 2014) (Fig. 1 site map).

Based on limited surveying, Winberry et al. (2014) estimated that the sticky spot extends ∼25 km and is likely elongated in the direction of flow, spanning approximately 500 km^2 in area. In light of the significance of the central sticky spot in this complex and evolving system, we initiated geophysical investigations to characterize it more thoroughly. First, using an aggregation of ice-thickness observations, we show that the sticky spot is associated with a broad subglacial high that likely directs subglacial water flow around rather than over the sticky spot. Results of our seismic reflection survey confirm that the resulting water diversion has created relatively strong subglacial sediment that contributes to the unique stick-slip behavior of the WIS.

2. Improved observations of bed topography and subglacial hydrologic potential

Previous work (Winberry et al., 2011, 2014) suggested that the present geometry of the ice stream and bed diverts water around the central sticky spot. The implication is that the sticky spot arises from relatively inefficient lubrication. However, previous inferences on subglacial water flow were hampered by relatively poor spatial coverage as well as large navigational uncertainties. To help alleviate these issues, we used new airborne radar observations from the Center for the Remote Sensing of Ice Sheets (CReSIS) to produce new maps of basal topography and hydraulic potential.

CReSIS flight lines over the study area have a nominal spacing of 1 km (Fig. 1e). Using these new observations, together with the relevant geophysical measurements that underlie Bedmap2 (Fretwell et al., 2013), we produced an updated regional-scale map of bed topography for the study area with greatly reduced absolute and relative uncertainties in the bed topography. Bedmap2 estimated basal topography by interpolating to a 5 km grid, then resampling at 1 km for publication. The data coverage here allows for a higher resolution gridding process. We interpolated the data at 1 km, smoothed the results with a 3 km mean filter, and validated the final grid using the original point data. With agreement between the grid and point observations, relative uncertainty in bed elevation near the CReSIS flight lines is simply the range resolution of the system (0.5 m; Wang et al., 2014). Additional absolute uncertainty is introduced by our choice of ice permittivity (3.15), but this has little effect on the computed hydropotential gradients. Through the gridding process, we ensure that no small-scale features that would affect our hydropotential analysis are smoothed away. For additional information, see Appendix A.

This new map shows that the sticky spot is associated with a broad topographic high (Fig. 1). As expected from the physics of ice flow (Whillans and Johnsen, 1983), the downglacier slope of the ice–air surface is relatively steep over the crest of the basal topographic high, providing the enhanced driving stress necessary to balance the additional basal resistance at the sticky spot.

Fast glacier motion is most often associated with the availability of subglacial water to promote basal sliding and till deformation. The routing of water from upstream likely plays a significant role in the ability of an ice stream to maintain rapid motion (e.g., Anandakrishnan and Alley, 1997; Parizek et al., 2002). To ascertain the significance of the newly discovered basal high in the delivery of subglacial water, we calculated the hydrostatic hydraulic potential φ beneath the WIS, assuming near-zero effective pressure:

$$\Phi = \rho_i g z_s + (\rho_w - \rho_i) g z_b \quad (1)$$

where ρ_i and ρ_w are the densities of ice and water respectively, g is acceleration due to gravity, and z_s and z_b are the ice sheet surface and bed elevations respectively (Shreve, 1972). The magnitude of Φ is plotted in Fig. 1d, with water flow paths down the potential gradient overlaid.

The results show that subglacial water is diverted around the sticky spot, with little or no upglacier supply reaching the center and downstream side of the sticky spot, if effective pressure on the sticky spot is similar to values elsewhere. (As discussed below, some water may reach the sticky spot at a higher effective pressure during slip events.)

3. Seismic reflection methods

Seismic data provide further insights on the basal conditions of the sticky spot. In Section 3.1, we explain the methodology we used to acquire, process, and interpret seismic reflection data. We focused on measuring the extent and thickness of the till across the sticky spot, and estimating its elastic properties. We first performed an analysis of the reflections from the base of the ice and the till in order to estimate the compressional-wave velocity (p-wave) and the thickness of the till. Then, we used the angular variation of reflection strength from the ice-bed interface (Aki and Richards, 1980) to estimate the velocity and density of the till.

3.1. Seismic data collection

During the 2011–2012 field season, a 10-km-long reflection seismic line was collected on the sticky spot, extending downglacier along the centerline of the sticky spot from near the high point of the basal topography. The receiver array consisted of 60 geophones spaced at 10 m. This array was moved along the line, and at each deployment ("spread location") two sources were initiated at 310 m and 460 m from the nearest geophone, and along the main line. In addition, two more "far-offset" shots were initiated at 1210 m and 1810 m distances, resulting in data with four images of each point along the line (so-called 4-fold data) for the whole profile. Additional near-offset shots were collected at 10 m and 160 m offset, but proved to have little utility because of high surface-wave energy ("ground-roll noise"). As discussed further below, this samples the bed at angles ranging from ∼15–60°. Explosive charges of 400 g of PETN (pentaerythritol tetranitrate) explosive were detonated in holes drilled to 20 m using a hot water drill, in order to keep the source amplitude consistent across the survey. The geophones were planted under approximately one meter of snow to reduce surface noise.

Seismic data were processed using standard techniques (Yilmaz, 2001). Frequency-wavenumber (FK) filtering was used to attenuate the direct-wave and ground-roll energy, which otherwise interfere with the bed reflection. Predictive and spiking deconvolution were applied to remove energy from short-path multiples and improve the coherence of the seismic record. Our seismic data have their primary energy at frequencies of ∼20–200 Hz, giving vertical resolution of approximately 5 m in ice.

3.2. Till thickness measurements

Next, we estimated the thickness and seismic velocity of the till from analysis of the shot gather data. We picked the arrival time of the ice and till-bottom reflectors (Fig. 2a). Using the normal moveout equation relating travel time to source–receiver offset, we estimated the reflection travel time at zero offset and the normal moveout velocity of those reflectors (Yilmaz, 2001). The seismic velocity of the till can then be calculated from the Dix (1955) equation:

$$V_{\text{int}} = \sqrt{\frac{V_{\text{tb}}^2 T_{\text{tb}} - V_{\text{ib}}^2 T_{\text{ib}}}{T_{\text{tb}} - T_{\text{ib}}}} \tag{2}$$

Here V_{tb} and T_{tb} are the normal-moveout velocity and time at zero offset, respectively, for the till bottom, and V_{ib} and T_{ib} are the velocity and time at zero offset for the ice bottom.

Seismic velocities and thicknesses were estimated from shots with high signal-to-noise ratio and a strong till bottom reflector. Strong reflectors were evident from the basal interfaces of both ice and till along the entire line. The till averages approximately 6 m thick with only small variations; velocities in the till range from ∼1950 to 2350 m s^{-1} with uncertainties of ∼200 m s^{-1} (Fig. 2b). Our uncertainties are relatively small in part because we have high signal-to-noise ratio (picking to within one sample or 0.5 ms), our cable had molded takeouts so that when dragged taut the offsets were accurate to better than 0.5 m, our sampling over middle to far offsets allows more-accurate estimates (Sheriff and Geldart, 1995), the bed is relatively flat and the ice homogeneous, and we averaged 40 measurements of travel time for each normal moveout velocity determination.

3.3. Till properties: Amplitude-Variation-with Offset

We apply the seismic Amplitude-Variation-with-Offset (AVO) technique to the ice-bottom reflection to learn basal properties along our seismic profile. AVO uses the angular dependence of amplitude and phase of the reflected wave to accurately characterize the contrast in material properties across an interface (Aki and Richards, 1980). Because ice has well-known seismic velocity and density, the AVO measurement of the contrast across the ice-till interface yields the till properties accurately.

The observed displacement amplitude (A) recorded at a surface geophone from a reflected seismic wave is given by Peters (2009):

$$A(\theta_{\text{i}}) = A_0 R(\theta_{\text{i}}) \gamma(\theta_{\text{i}}) e^{-ar(\theta_{\text{i}})} \tag{3}$$

where $r(\theta_{\text{i}})$ is the raypath distance from source to receiver for a particular incidence angle θ_{i}, R is the reflection coefficient of the interface, γ accounts for geometric spreading, a is the attenuation (0.2 km^{-1}, Bentley and Kohenen, 1976), and A_0 is the source amplitude.

The reflection coefficient, R, can be calculated from observed amplitudes using equation (3). R depends on the contrast in seismic velocity (compressional wave velocity (V_{p}), shear wave velocity (V_{s})) and density (ρ) across an interface, with a dependence on angle θ_{i} as represented in the Zoeppritz equations (Aki and Richards, 1980). Substrates likely to be in contact with ice (e.g., dilated till, lodged till, sedimentary rock) yield quite different patterns of reflection polarity and amplitude as a function of incidence angle (Peters et al., 2007).

AVO analysis uncertainties decrease as the range of measured angles increases. Logistical and time constraints limited our experiment to angles ranging from approximately 15 to 60° (310–2400 m offsets). During processing of the data we noted that the bed is relatively homogeneous at scales of 500 m to 1 km. We thus combined multiple reflecting points into a single "super-gather" that has a larger range of angles of incidence than would be possible at any single reflection point to obtain a complete snapshot of angles from 15 to 60°. Of these, the angles with low SNR were omitted in the final AVO analysis. The loss of horizontal resolution is acceptable because of the relatively uniform bed.

Amplitudes of the bed reflection are used to compute reflection coefficients. The signal to noise ratio (SNR) was estimated by comparing the peak of the reflection from the bed to the energy in a 5 ms window before the bed reflection arrival (assumed to be a measure of background noise). Receivers with low SNR were excluded from the AVO analysis. In general, receivers close to the source (up to 500 m offset) were most affected by source-generated noise. In Figs. 3 and 4, the gaps in data coverage arise partly from our SNR thresholding. Because of the logistical constraints, our data have a gap in coverage from angles of 35 to 40° (corresponding to offsets of 1050–1200 m).

Next, the amplitudes were corrected for variations in strength and coupling of the source and in receiver coupling. The chemical sources have natural variability in their yield; in addition, the shotholes at approximately 20 m depth likely were in snow of

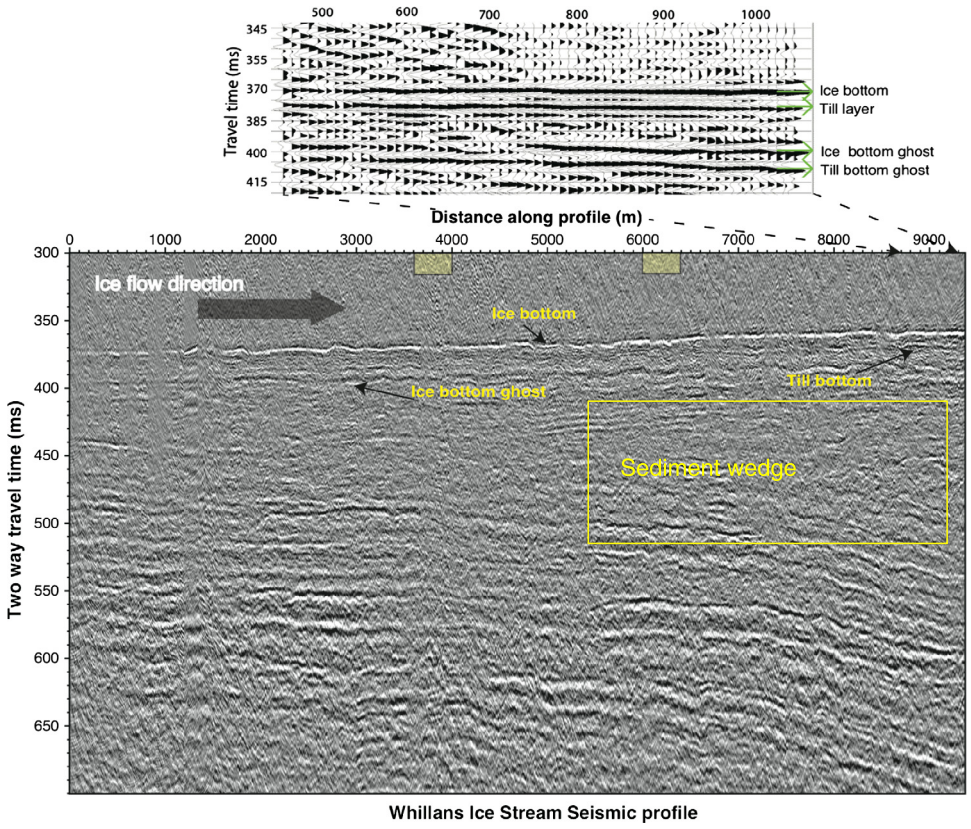

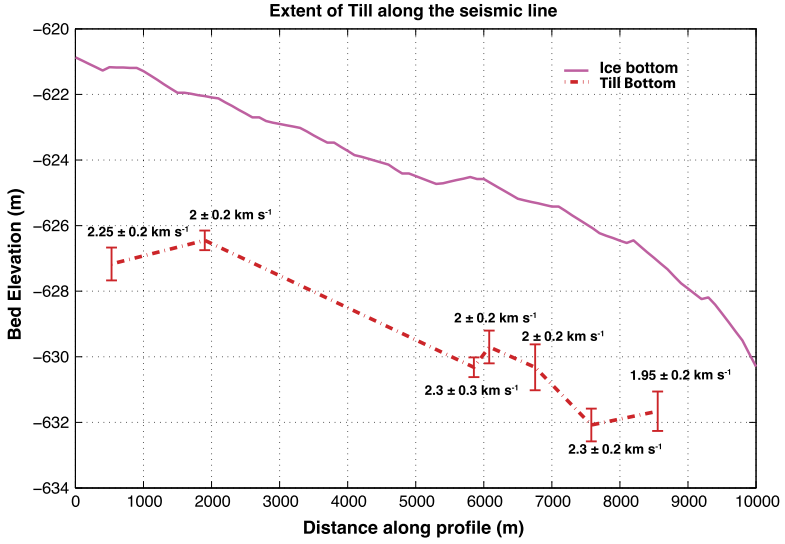

Fig. 2. a) Travel-time seismic profile. The yellow boxes mark the sections of the bed where AVO analysis was carried out. The inset (top) shows a NMO corrected shot gather from near the downstream end of the line, with the ice and till bottoms labeled. b) The profile of 2a, plotted with depth rather than travel time, shows ice bottom, till bottom with uncertainty (1-sigma), and numerical values of interval velocities. (For interpretation of the references to color in this figure legend, the reader is referred to the web version of this article.)

varying density, affecting their coupling. Geophones were planted by hand and allowed to sinter for varying amounts of time, which affected their sensitivity to seismic waves. We accounted for these effects by measuring the direct wave amplitude, which is unaffected by bed properties and is most sensitive to source size and source coupling. These measurements were used to correct the bed reflection (Peters, 2009). Finally, a standard estimate for geometrical spreading loss based on the raypath length was used to normalize the amplitudes. These corrections allowed us to compare the observed reflectivities along the line as calculated using Equation (3).

As noted above, the angular dependence of reflection phase and amplitude depends on the contrast in density and seismic velocities across the interface, as given in the Zoeppritz equations. We used a four-layer firn velocity model to determine the seismic velocity of ice, and our results are fully consistent with expectations from prior work ($V_p = 3840\ \mathrm{m\,s^{-1}}$, $V_s = 1860\ \mathrm{m\,s^{-1}}$ and density $= 920\ \mathrm{kg\,m^{-3}}$ (Christensen, 1989; Peters et al., 2007)). We used a least-squares minimization technique to search for the till properties that best match the observations. The best fit, together with results for bracketing till properties, are shown in Figs. 3 and 4 for the two 400-m sections of the bed.

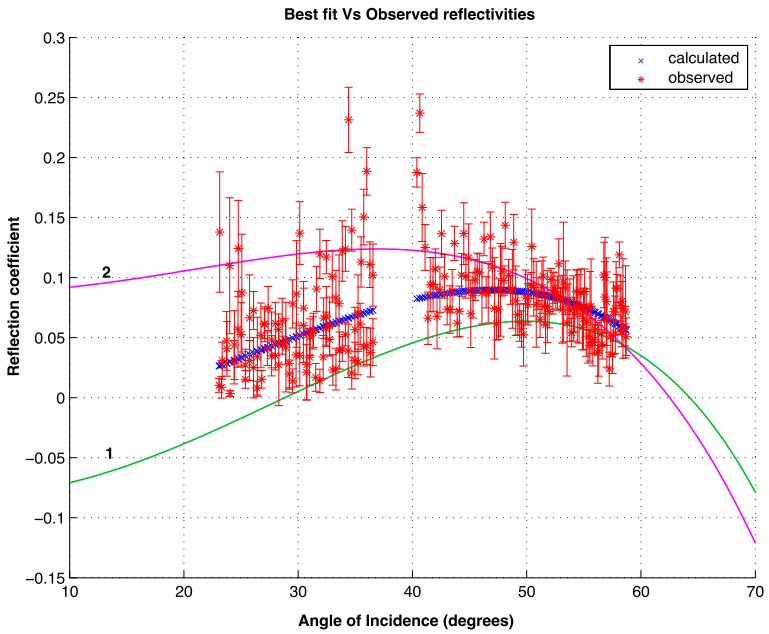

Fig. 3. Basal reflection coefficient and uncertainty (1-sigma) against incidence angle, for section from 3600 to 4000 m. The blue line shows the least squares fit for the observed reflection coefficients ($V_p = 1840\ \mathrm{m\,s^{-1}}$, $V_s = 310\ \mathrm{m\,s^{-1}}$, density $= 1835\ \mathrm{kg\,m^{-3}}$). To illustrate sensitivity of the inversion to the parameters, lines 1 and 2 are forward model curves based on the Zoeppritz equations: 1. $V_p = 1730\ \mathrm{m\,s^{-1}}$, $V_s = 250\ \mathrm{m\,s^{-1}}$, density $= 1730\ \mathrm{kg\,m^{-3}}$; 2. $V_p = 2050\ \mathrm{m\,s^{-1}}$, $V_s = 500\ \mathrm{m\,s^{-1}}$, density $= 2050\ \mathrm{kg\,m^{-3}}$. (For interpretation of the references to color in this figure legend, the reader is referred to the web version of this article.)

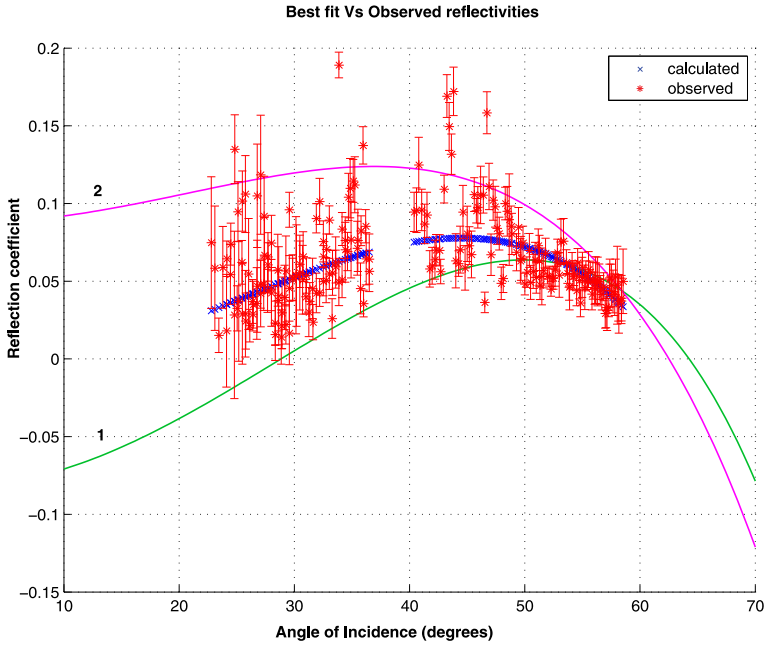

Fig. 4. As in Fig. 3, basal reflection coefficient and uncertainty (1-sigma) against incidence angle, for section from 6000 to 6400 m. The blue line shows the least squares fit for the observed reflection coefficients ($V_p = 1860\ \mathrm{m\,s^{-1}}$, $V_s = 370\ \mathrm{m\,s^{-1}}$, density $= 1870\ \mathrm{kg\,m^{-3}}$). Lines 1 and 2 are forward model curves based on the Zoeppritz equations: 1. $V_p = 1730\ \mathrm{m\,s^{-1}}$, $V_s = 250\ \mathrm{m\,s^{-1}}$, density $= 1730\ \mathrm{kg\,m^{-3}}$; 2. $V_p = 2050\ \mathrm{m\,s^{-1}}$, $V_s = 500\ \mathrm{m\,s^{-1}}$, density $= 2050\ \mathrm{kg\,m^{-3}}$. (For interpretation of the references to color in this figure legend, the reader is referred to the web version of this article.)

4. Seismic results and interpretation

4.1. Seismic reflection

The seismic image of Whillans Ice Stream is shown in Fig. 2a, with important features labeled. The "ghost" arises from energy propagating upward from the approximately 20-m-deep shots to the surface, reflecting, and then following the energy initially propagating downward from the shot. The bed of the ice stream is relatively flat, and produces a strong reflection along the entire profile. High ground-roll noise from near-offset shots (10 and 160 m away from source) reduced data quality in the upstream 1 km of the line; subsequently, the shooting spread was switched to 310 and 460 m from the source, and data quality improved notably.

The seismic image shows several hundred meters of sedimentary layers beneath the ice. Reflections from within deeper sediments are evident, and suggest an interesting structural and depositional history, which we plan to explore in greater detail in a separate contribution. Slight post-depositional folding appears to have occurred, perhaps over a subsurface fault not imaged here,

Table 1
Seismic properties of the till inferred from AVO analysis with uncertainty (1-sigma).

	Section (m)	
	3600–4000	6000–6400
V_p ($m\,s^{-1}$)	1840 ± 180	1860 ± 160
V_s ($m\,s^{-1}$)	310 ± 34	370 ± 80
Density ($kg\,m^{-3}$)	1835 ± 180	1870 ± 190
Porosity	0.37 ± 0.1	0.36 ± 0.1

with the sticky spot on the upthrown side, and the downthrown side in the downglacier direction, suggesting that the sticky spot is structurally controlled. A sedimentary wedge appears to have been deposited in the lee of the sticky spot.

In this contribution, we focus on the existence and characteristics of the few-meter-thick layer at the top of the sedimentary sequence in contact with the ice. By analogy to the seismic results from Blankenship et al. (1986) and subsequent work, the borehole observations of Engelhardt and Kamb (1998) and Tulaczyk et al. (2000), and additional information, we identify this as a till layer unconformably overlying the older sediments. As discussed below, our evidence suggests that this till is deforming, much like behavior elsewhere beneath the fast-moving Siple Coast ice streams, despite the better drained character of the sticky spot.

4.2. Till thickness and seismic interval velocity

The till thickness is mapped along our seismic line in Fig. 2b. We find an average of 6 ± 0.5 m, comparable to the 6.5 ± 0.5 m found by Rooney et al. (1987) farther upstream on WIS. The till is thinned slightly near 2500 m on the profile, over a local high spot in the bed (inset of Fig. 1).

Interval velocities for p-waves in till, V_p, are given in Fig. 2b. We note that our seismic configuration did not produce sufficient shear-wave energy to allow confident picking of arrivals, unlike the work of Blankenship et al. (1986, 1987).

The average of the seven estimates is $V_p = 2120\ m\,s^{-1}$; with the uncertainties (1-sigma) of about $200\ m\,s^{-1}$ on individual determinations, there are no significant differences in seismic velocity along the seismic line. However, the velocities are significantly higher than found in prior work on well-lubricated parts of Siple Coast ice streams. Blankenship et al. (1986), for example, found $V_p = 1600 \pm 150\ m\,s^{-1}$.

The strong positive polarity of the ice bottom reflection along the entire line is consistent with the relatively high seismic velocity of the till, together with a relatively high till density. Note that we sampled the bed at 15–60° incidence angles, not at vertical incidence; our estimated till properties would yield a weak reflection at vertical incidence. In well-lubricated ice-stream regions, the reflection coefficient is small, and both positive and negative phases are observed (Atre and Bentley, 1993); our higher acoustic impedance (velocity multiplied by density) yields the positive-phase reflection. This is explored further in the next section.

4.3. AVO analysis

As noted above, the angular dependence of the phase and amplitude of seismic reflections from an interface depends on the contrast in p-wave velocity, s-wave velocity and density across the interface. We performed the AVO analysis on two separate 400 m long sections of the ice stream bed, at the locations indicated in Fig. 2a. The best-fit inversion results are shown in Figs. 3 and 4, and the numerical values are listed in Table 1. There are no statistically significant differences in seismic wave velocities or densities between the two regions.

The best-fit V_p values from AVO are lower than those found in the interval velocity. The uncertainties overlap, so strong conclusions cannot be drawn, but this difference is as expected if the till is actively interacting with the moving ice. AVO is sensitive primarily to conditions in the top $\sim 1/4$ wavelength (Peters et al., 2007), which for 100 Hz and 450 $m\,s^{-1}$ shear wave velocity is ~1.5 m. The deforming till beneath well-lubricated parts of the Siple Coast ice streams is generally softer and more dilated toward the top than toward the bottom (Kamb, 2001), so the interval velocities averaging over the whole till thickness is expected to sample a somewhat more-consolidated material and thus to be higher than the AVO velocities sampling the upper part if the upper part is deforming. The offset between the central estimates for the interval and AVO velocities in our data appears to be larger than expected from the small downward increase in effective pressure caused by the difference between hydrostatic and lithostatic stresses (Blankenship et al., 1987).

4.4. Estimate for porosity and effective pressure

Various efforts have been made to estimate glaciologically important parameters such as effective pressure (overburden pressure minus water pressure) and till porosity from seismic or borehole observations (Blankenship et al., 1986, 1987; Kamb, 2001; Tulaczyk et al., 2001a). Those based primarily on seismic data suffer from uncertainty linked to differences between calibration samples and the *in situ* materials. Regardless of the technique, though, our data are indicative of significantly higher effective pressure, lower porosity, and overall stiffer till than in the well-lubricated, fast-moving parts of the ice stream (Blankenship et al., 1986, 1987; Kamb, 2001; Tulaczyk et al., 2001a). We provide one estimate of the difference in Appendix B, based on the technique of Dvorkin et al. (1999), and yielding an effective pressure from our AVO results 10–40 kPa higher than for Blankenship et al. (1986, 1987), despite our data sampling a shallower part of the till, biasing our measurement toward lower effective pressure.

5. Discussion

Our data show that the main sticky spot on the ice plain of WIS has a few-meters-thick, continuous till layer overlying older sediments. Comparison of the AVO results (which sample the upper part of the till) to the interval velocities (which average through the till) suggests that the upper part of the till is softer (higher porosity, lower effective pressure) than the deeper part. Comparison to prior seismic (Blankenship et al., 1986, 1987) and borehole (Kamb, 2001; Tulaczyk et al., 2001a) data shows that the till beneath well-lubricated parts of the ice stream is softer than the till in our study. In other ways, though, our data suggest that the sticky spot is similar to adjacent, better-lubricated parts of WIS and adjacent ice streams in having active deformation of a few-meters-thick, continuous till layer unconformably overlying older sedimentary rocks.

We note that direct borehole confirmation of our results would be valuable, as would additional geophysical observations. However, strong constraints on likely conditions are provided by our new observations together with the prior seismic and borehole observations.

In light of the large unsteadiness on the Siple Coast (Hulbe and Fahnestock, 2007), one possibility is that the till on the sticky spot was emplaced sometime before the sticky spot formed, and ceased deforming as the sticky spot developed. Because the ice flowlines continue across the sticky spot, till continuity together with the indications of till deformation beneath well-lubricated parts of the ice stream (e.g., Kamb, 2001) would then indicate that the subglacial till flux is accumulating near the upglacier end of the sticky

spot, likely with erosion at the downglacier end; our seismic line is not long enough to observe the probable locations of any such changes.

Our data are more consistent with ongoing deformation of the till across the sticky spot, however. Recall that the till appears to be softer at the top. It is likely that any deformation is localized there, rather than having jumped downward to a shear plane in stiffer till beneath. Localized motion near the top of the till would allow the ice-till interface to provide a pathway for water drainage, as is usual beneath glaciers and ice sheets with thawed beds and as was observed elsewhere beneath WIS (e.g., Kamb, 2001). Following Tulaczyk et al. (2000), if deformation of the till ceased, dewatering to the ice-till interface would cause compaction to propagate downward, but we see softer rather than more-compacted till at the top. We cannot entirely exclude the possibility that compaction of the uppermost till has started so recently that it has not produced a seismically detectable layer, but it seems more likely that the upper part of the till remains notably softer than the deeper part because deformation is concentrated in the upper part.

Our data show that the till layer is continuous, and thus must support the shear stress of the ice. Because the sticky spot supports a higher shear stress than surrounding regions during the "stick" part of the stick-slip motion of WIS (Winberry et al., 2009), the till on the sticky spot must be stiffer than elsewhere, as observed. Deformation during slip events to maintain the vertical contrast in the till could involve relatively deep ploughing (Brown et al., 1987; Tulaczyk et al., 2001b), localized sliding on discrete planes that move during or between events, or more pervasive deformation; the seismic technique cannot easily distinguish between such possibilities.

The hydrological potential gradient calculated assuming spatially uniform effective pressure directs water away from the sticky spot. Thus, one might expect that the till would become progressively dewatered along flow, but we do not observe any significant trends in till properties that would arise from such dewatering along our seismic line. One possibility is that water generation from the heat of sliding on the sticky spot provides a new supply; freeze-on generally occurs on the well-lubricated parts of the Siple Coast ice streams (Kamb, 2001), but the higher shear stress yet similar velocity on the sticky spot would favor basal melting.

Water also might be diverted onto the sticky spot due to higher effective pressure (relatively lower water pressure) at the ice-till interface there, as is suggested by the seismic results showing stiffer till on the sticky spot. Weertman (1972) (also see Alley, 1993) suggested that the water pressure in a distributed system is lowered below the overburden pressure by an amount that is proportional to the basal shear stress, with a constant of proportionality of order 1, because higher shear stress causes larger variations in normal stress on the bed, and water preferentially flows in the lower pressure regions. Probably more importantly, much larger water-pressure drops may be generated transiently in lee-side cavities during seismic motion events, if notable displacement occurs between the ice and the substrate (Zoet et al., 2013), pumping water into the fault zone from surroundings. This suction pump action at dilational fault jogs is known from tectonic faults (Sibson, 1985).

We recognize that other interpretations of our data are possible, if the full range of uncertainties is considered, and we encourage borehole or additional geophysical and model testing of our hypotheses. Pending this, our data provide a consistent picture of the most-likely behavior. The stiffer till in the sticky spot fails under the higher shear stresses that accumulate there before motion events. Motion may be localized between ice and till but extends into the till, decreasing with increasing depth. A quasi-steady state exists in which till and some water are transported subglacially across the sticky spot, with water transferred from surrounding regions onto the sticky spot in response to pressure drop in lee-side cavities (dilational fault jogs) during motion events.

6. Conclusions

Radar, seismic and GPS observations show that the main sticky spot of the ice plain of Whillans Ice Stream, West Antarctica, is a local surface high controlled by a higher-amplitude bedrock high composed of sedimentary rocks with possible structural control. The bedrock high is mantled by a seismically distinct layer, which we assume to be till based on nearby observations and physical understanding (Kamb, 2001), that has a relatively uniform thickness of approximately 6 m. AVO seismic data, primarily sampling the upper part of the till, and interval velocities averaged over the whole thickness, show that the entire seismically detectable package is more consolidated (higher density, lower porosity, higher p-wave and s-wave velocities, higher effective pressure) than the corresponding till beneath well-lubricated parts of the ice stream; consolidation likely increases downward in the till similar to behavior in well-lubricated regions. The vertical consolidation profile suggests that the till continues to deform with the ice, perhaps aided by water pumping into lee-side cavities during seismic motion events. Analogy of the sticky spot, till, and seismic motion events of WIS to asperities and fault gouge of tectonic earthquake faults suggests that additional studies targeting this feature could be of both glaciological and broader interest.

Acknowledgements

This work was funded by grants from the U.S. NSF Office of Polar Programs through the Whillans Stick-Slip (0944286), CReSIS (0852697), and WISSARD (0838764, 0838763) projects. Raytheon Polar Services and The New York Air National Guard provided logistical support. The IRIS-PASSCAL Instrument Center and Ice Drilling Design and Operations provided equipment essential to the success of the project. We thank Martin Pratt, Angela Hoffer, Huw Horgan and Matthew Siegfried for help with data acquisition during the 2011–2012 field season.

Appendix A. Supplementary material

Supplementary material related to this article can be found online at http://dx.doi.org/10.1016/j.epsl.2016.01.035.

References

Aki, K., Richards, P.G., 1980. Quantitative Seismology: Theory and Methods, vol. 1. WH Freeman Co.

Alley, R.B., Blankenship, D.D., Bentley, C.R., Rooney, S.T., 1986. Deformation of till beneath ice stream B, West Antarctica. Nature 322, 57–59.

Alley, R.B., Blankenship, D.D., Bentley, C.R., Rooney, S.T., 1987. Till beneath ice stream B: 3. Till deformation: evidence and implications. J. Geophys. Res. 92. http://dx.doi.org/10.1029/JB092iB09p08921.

Alley, R.B., 1993. In search of ice-stream sticky spots. J. Glaciol. 39 (133), 447–454.

Anandakrishnan, S., Alley, R.B., 1997. Stagnation of ice stream C, West Antarctica by water piracy. Geophys. Res. Lett. 24, 265–268.

Atre, S.R., Bentley, C.R., 1993. Laterally varying basal conditions beneath Ice Streams B and C, West Antarctica. J. Glaciol. 39, 507–514.

Bamber, J.L., Riva, R.E.M., Vermeersen, B.L.A., LeBrocq, A.M., 2009. Reassessment of the potential sea-level rise from a collapse of the West Antarctic Ice Sheet. Science 324, 901–903.

Beem, L.H., Tulaczyk, S.M., King, M.A., Bougamont, M., Fricker, H.A., Christoffersen, P., 2014. Variable deceleration of Whillans Ice Stream, West Antarctica. J. Geophys. Res., Earth Surf. 119, 212–224. http://dx.doi.org/10.1002/2013JF002958.

Bentley, C.R., Kohnen, H., 1976. Seismic refraction measurements of internal friction in Antarctic ice. J. Geophys. Res. 81 (8), 1519–1526. http://dx.doi.org/10.1029/JB081i008p01519.

Bindschadler, R.A., King, M.A., Alley, R.B., Anandakrishnan, S., Padman, L., 2003. Tidally controlled stick-slip discharge of a West Antarctic ice. Science 301, 1087–1089.

Blankenship, D.D., Bentley, C.R., Rooney, S.T., Alley, R.B., 1986. Seismic measurements reveal a saturated porous layer beneath an active Antarctic ice stream. Nature 322, 54–57.
Blankenship, D.D., Bentley, C.R., Rooney, S.T., Alley, R.B., 1987. Till beneath Ice Stream B: 1. Properties derived from seismic travel times. J. Geophys. Res., Solid Earth 92, 8903–8911.
Brown, N.E., Hallet, B., Booth, D.B., 1987. Rapid soft bed sliding of the Puget glacial lobe. J. Geophys. Res., Solid Earth 92, 8985–8997.
Christensen, N.I., 1989. Seismic velocities. In: Carmichael, R.S. (Ed.), CRC Practical Handbook of Physical Properties of Rocks and Minerals. CRC Press, Boca Raton, FL, pp. 429–546.
Clarke, G.K.C., 1987. Fast glacier flow: Ice streams, surging, and tidewater glaciers. J. Geophys. Res. 92. http://dx.doi.org/10.1029/JB092iB09p08835.
Dix, C.H., 1955. Seismic velocities from surface measurements. Geophysics 20, 68–86.
Dvorkin, J., Prasad, M., Sakai, A., Lavoie, D., 1999. Elasticity of marine sediments: rock physics modeling. Geophys. Res. Lett. 26, 1781–1784.
Engelhardt, H., Kamb, B., 1998. Basal sliding of ice stream B, West Antarctica. J. Glaciol. 44, 223–230.
Engelhardt, H., Kamb, B., 2013. Kamb Ice Stream flow history and surge potential. Ann. Glaciol. 54, 287–298.
Fretwell, P., Pritchard, H.D., Vaughan, D.G., Bamber, J.L., Barrand, N.E., Bell, R., Bianchi, C., Bingham, R.G., Blankenship, D.D., Casassa, G., 2013. Bedmap2: improved ice bed, surface and thickness datasets for Antarctica. Cryosphere 7.
Hulbe, C., Fahnestock, M., 2007. Century-scale discharge stagnation and reactivation of the Ross ice streams, West Antarctica. J. Geophys. Res. 112. http://dx.doi.org/10.1029/2006JF000603.
Jacobs, S.S., Jenkins, A., Giulivi, C.F., Dutrieux, P., 2011. Stronger ocean circulation and increased melting under Pine Island Glacier ice shelf. Nat. Geosci. 4, 519–523.
Joughin, I., Bindschadler, R.A., King, M.A., Voigt, D., Alley, R.B., Anandakrishnan, S., Horgan, H., Peters, L., Winberry, P., Das, S.B., 2005. Continued deceleration of Whillans Ice Stream, West Antarctica. Geophys. Res. Lett. 32.
Joughin, I., Alley, R.B., 2011. Stability of the West Antarctic ice sheet in a warming world. Nat. Geosci. 4, 506–513.
Joughin, I., Smith, B.E., Medley, B., 2014. Marine ice sheet collapse potentially under way for the Thwaites Glacier Basin, West Antarctica. Science 344, 735–738. http://dx.doi.org/10.1126/science.1249055.
Kamb, B., 2001. Basal zone of the West Antarctic ice streams and its role in lubrication of their rapid motion. In: West Antarctic Ice Sheet: Behavior and Environment. In: Antarct. Res. Ser., vol. 77. American Geophysical Union, pp. 157–199.
MacAyeal, D.R., 1989. Large-scale ice flow over a viscous basal sediment: theory and application to ice stream B, Antarctica. J. Geophys. Res., Solid Earth 94, 4071–4087.
Parizek, B.R., Alley, R.B., Anandakrishnan, S., Conway, H., 2002. Sub-catchment melt and long-term stability of ice stream D, West Antarctica. Geophys. Res. Lett. 29, 51–55.
Peters, L.E., Anandakrishnan, S., Alley, R.B., Smith, A.M., 2007. Extensive storage of basal meltwater in the onset region of a major West Antarctic ice stream. Geology 35. http://dx.doi.org/10.1130/g23222a.1.
Peters, L.E., 2009. A seismic investigation of basal conditions in glaciated regions. PhD thesis. The Pennsylvania State University.
Pratt, M.J., Winberry, J.P., Wiens, D.A., Anandakrishnan, S., Alley, R.B., 2014. Seismic and geodetic evidence for grounding-line control of Whillans Ice Stream stick-slip events. J. Geophys. Res., Earth Surf. 119, 333–348. http://dx.doi.org/10.1002/2013JF002842.
Raymond, C.F., Echelmeyer, K.A., Whillans, I.M., Doake, C.S.M., 2001. Ice stream shear margins. In: The West Antarctic Ice Sheet: Behavior and Environment. In: Antarct. Res. Ser., vol. 77. American Geophysical Union, pp. 137–155.
Rignot, E., Mouginot, J., Scheuchl, B., 2011. Ice flow of the Antarctic ice sheet. Science 333, 1427–1430.
Rignot, E., Mouginot, J., Morlighem, M., Seroussi, H., Scheuchl, B., 2014. Widespread, rapid grounding line retreat of Pine Island, Thwaites, Smith and Kohler glaciers, West Antarctica from 1992 to 2011. Geophys. Res. Lett. http://dx.doi.org/10.1002/2014GL060140.
Rooney, S.T., Blankenship, D.D., Bentley, C.R., Alley, R.B., 1987. Till Beneath Ice Stream B 2. Structure and continuity. J. Geophys. Res. 92, 8913–8920.
Sheriff, R.E., Geldart, L.P., 1995. Exploration Seismology. Cambridge University Press.
Shreve, R.L., 1972. Movement of water in glaciers. J. Glaciol. 11, 205–214.
Sibson, R.H., 1985. A note on fault reactivation. J. Struct. Geol. 7, 751–754.
Tulaczyk, S., Kamb, W.B., Engelhardt, H.F., 2000. Basal mechanics of Ice Stream B, West Antarctica: 2. Undrained plastic bed model. J. Geophys. Res., Solid Earth 105, 483–494.
Tulaczyk, S., Kamb, B., Engelhardt, H.F., 2001a. Estimates of effective stress beneath a modern West Antarctic ice stream from till preconsolidation and void ratio. Boreas 30, 101–114. http://dx.doi.org/10.1080/030094801750203134.
Tulaczyk, S.M., Scherer, R.P., Clark, C.D., 2001b. A ploughing model for the origin of weak tills beneath ice streams: a qualitative treatment. Quat. Int. 86, 59–70.
Walker, R.T., Parizek, B.R., Alley, R.B., Anandakrishnan, S., Riverman, K.L., Christianson, K., 2013. Ice-shelf tidal flexure and subglacial pressure variations. Earth Planet. Sci. Lett. 361, 422–428.
Wang, Z., Gogineni, S., Rodriguez-Morales, F., Yan, J.-B., Hale, R., Paden, J., Leuschen, C., Carabajal, C., Gomez-Garcia, D., Townley, B., 2014. Wideband imaging radar for cryospheric remote sensing. In: 2014 IEEE International Geoscience and Remote Sensing Symposium, IGARSS. IEEE, pp. 4026–4029.
Weertman, J., 1972. General theory of water flow at the base of a glacier or ice sheet. Rev. Geophys. 10, 287–333.
Whillans, I.M., Johnsen, S.J., 1983. Longitudinal variations in glacial flow: theory and test using data from the Byrd Station strain network, Antarctica. J. Glaciol. 29, 78–97.
Wiens, D.A., Anandakrishnan, S., Winberry, J.P., King, M.A., 2008. Simultaneous teleseismic and geodetic observations of the stick–slip motion of an Antarctic ice stream. Nature 453, 770–774.
Winberry, J.P., Anandakrishnan, S., Alley, R.B., Bindschadler, R.A., King, M.A., 2009. Basal mechanics of ice streams: insights from the stick-slip motion of Whillans Ice Stream, West Antarctica. J. Geophys. Res. 114, 1–11. http://dx.doi.org/10.1029/2008JF001035.
Winberry, J.P., Anandakrishnan, S., Wiens, D.A., Alley, R.B., Christianson, K., 2011. Dynamics of stick–slip motion, Whillans Ice Stream, Antarctica. Earth Planet. Sci. Lett. 305. http://dx.doi.org/10.1016/j.epsl.2011.02.052.
Winberry, J.P., Anandakrishnan, S., Wiens, D.A., Alley, R.B., 2013. Nucleation and seismic tremor associated with the glacial earthquakes of Whillans Ice Stream, Antarctica. Geophys. Res. Lett. 40, 312–315. http://dx.doi.org/10.1002/grl.50130.
Winberry, J.P., Anandakrishnan, S., Alley, R.B., Wiens, D.A., Pratt, M.J., 2014. Tidal pacing, skipped slips and the slowdown of Whillans Ice Stream, Antarctica. J. Glaciol. 60, 795–807.
Yilmaz, Ö., 2001. Seismic Data Analysis. Society of Exploration Geophysicists, Tulsa.
Zoet, L.K., Alley, R.B., Anandakrishnan, S., Christianson, K., 2013. Accelerated subglacial erosion in response to stick-slip motion. Geology 41, 159–162.